

Free-Breathing Multislice Native Myocardial T_1 Mapping Using the Slice-Interleaved T_1 (STONE) Sequence

Sebastian Weingärtner,^{1,2} Sébastien Roujol,¹ Mehmet Akçakaya,¹
Tamer A. Basha,¹ and Reza Nezafat^{1*}

Purpose: To develop a novel pulse sequence for free-breathing, multislice, native myocardial T_1 mapping.

Methods: The slice-interleaved T_1 (STONE) sequence consists of multiple sets of single-shot images of different slices, acquired after a single nonselective inversion pulse. Each slice is only selectively excited once after each inversion pulse to allow sampling of the unperturbed longitudinal magnetization in the adjacent slices. For respiratory motion, a prospective slice-tracking respiratory navigator is used to decrease through-plane motion followed by a retrospective image registration to reduce in-plane motion. STONE T_1 maps were calculated using both a two-parameter and three-parameter fit model. The accuracy and precision of the STONE sequence for different T_1 , T_2 , and inversion pulse efficiency were studied using numerical simulations and phantom experiments. T_1 maps from 14 subjects were acquired with the STONE sequence and T_1 s were compared to the Modified Look-Locker Inversion recovery sequence (MOLLI).

Results: In numerical simulations and phantom experiments, the STONE sequence using a two-parameter fit model yields more accurate T_1 times compared to MOLLI, with similar high precision. The three-parameter fit model further improves the accuracy, but with a reduced precision. The native myocardial T_1 times were higher in the STONE sequence using two- or three-parameter fit compared to MOLLI. The standard deviation of the T_1 times was lower in the STONE T_1 maps with a two-parameter fit compared with MOLLI or a three-parameter fit.

Conclusion: The STONE sequence allows accurate and precise quantification of native myocardial T_1 times with the additional benefit of covering the entire ventricle. **Magn Reson Med 000:000–000, 2014. © 2014 Wiley Periodicals, Inc.**

Key words: Myocardial T_1 mapping; inversion recovery; multislice; MOLLI

INTRODUCTION

Recent advances in cardiac MR (CMR) allow for the non-invasive imaging of interstitial diffuse fibrosis using quantitative T_1 mapping. In this technique, the voxel-wise calculation of the longitudinal magnetization recovery

time provides spatially-resolved quantitative characterization of the myocardial tissue composition. There is emerging evidence of differences in myocardial T_1 times between various cardiomyopathies, which may improve diagnostic and prognostic value of CMR (1). Both native and postcontrast myocardial T_1 times have been used to evaluate patients with various cardiomyopathies (2–6). Furthermore, extracellular volume (ECV) can be calculated by measuring native and postcontrast T_1 , taking into account the patient hematocrit (7).

Over the past decade, there have been significant advances in imaging sequences for myocardial T_1 mapping. The Modified Look-Locker (8) Inversion recovery (MOLLI) is widely used for myocardial T_1 mapping (9–13). However, it suffers from inaccurate T_1 estimates due to heart rate (14), T_2 (15), and magnetization transfer dependency (16). To reduce the scan time and eliminate heart rate variability, variations of the MOLLI sequence like the 5(3)3 MOLLI scheme (17) or the shortened MOLLI (ShMOLLI) were developed (14). However, these sequences still suffer from inaccurate measurements leading to underestimated T_1 of healthy myocardium by up to ~30% (18). Saturation recovery based myocardial T_1 mapping was also investigated (19) and recently revisited by introduction of the SATuration recovery single-SHOT Acquisition sequence (SASHA) (20). This sequence reduces sensitivity to T_2 and heart rate, but it has lower precision compared to MOLLI (18). SATuration Pulse-Prepared Heart-rate independent Inversion-REcovery (SAPPHIRE) T_1 mapping, uses a magnetization preparation using a combination of saturation and inversion pulses, for accurate T_1 mapping with an increased dynamic range compared to saturation recovery (21). Similar to SASHA, SAPPHIRE suffers from lower precision in assessing native T_1 times compared to MOLLI (18). Therefore, there is still a need for an accurate and precise T_1 mapping imaging sequence.

Myocardial T_1 mapping is frequently performed using a 2D sequence during breath-holds, with the acquisition of a single breath-hold per slice. The majority of published studies use a single mid left ventricular (LV) slice for the calculation of T_1 maps, and report a single T_1 time for each patient (6,22,23). However, a single value does not necessarily characterize the regional myocardial tissue composition over the entire ventricle. While in some myopathies such as amyloidosis, there may not be much variation across the myocardium, in many cardiomyopathies, such as hypertrophic cardiomyopathies, there are regional variations that could directly impact T_1 measurements (23,24). Therefore, full LV coverage is required for accurate characterization of the LV

¹Department of Medicine, Beth Israel Deaconess Medical Center and Harvard Medical School, Boston, Massachusetts, USA.

²Department of Computer Assisted Clinical Medicine, University Medical Center Mannheim, Heidelberg University, Mannheim, Germany.

Grant sponsor: NIH; Grant number: R01EB008743-01A2; Grant sponsor: Samsung Electronics.

*Correspondence to: Reza Nezafat, Ph.D., Beth Israel Deaconess Medical Center, 330 Brookline Avenue, Boston, MA, 02215. E-mail: rnezafat@bidmc.harvard.edu

Received 28 March 2014; revised 6 June 2014; accepted 4 July 2014

DOI 10.1002/mrm.25387

Published online 00 Month 2014 in Wiley Online Library (wileyonlinelibrary.com).

© 2014 Wiley Periodicals, Inc.

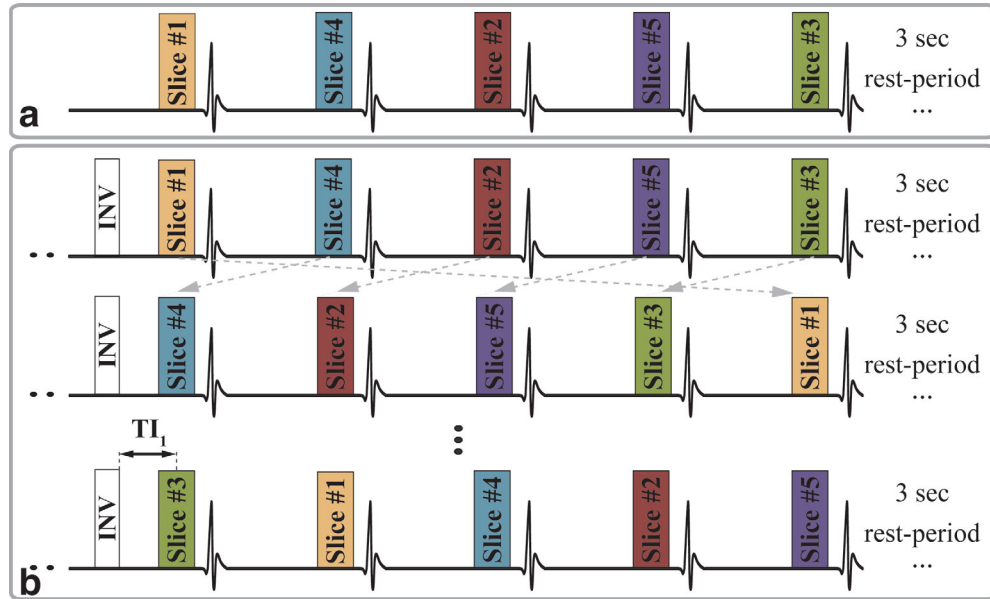


FIG. 1. Sequence scheme of the proposed STONE sequence, which is acquired over 85 heartbeats. The sequence consists of two steps. At the beginning of the scan shown in **a**, 5 images at different locations (i.e., slice #1 to #5) are acquired without any inversion pulse to enable the sampling of the fully recovered longitudinal magnetization. After a 3-s rest period, data acquisition is resumed by acquiring data for 5 slices after application of a single nonselective inversion pulse (INV) with a delay of T_{I1} as shown in **b**. This block is repeated after a 3-s rest period and the order of slices will be permuted. Finally, the imaging step shown in **B** is repeated with an adjusted inversion time (T_{I2}). Ultimately, this sequence yields 11 images for each slice corresponding to an inversion times of ∞ , T_{I1} , $T_{I1} + 1$ RR, $T_{I1} + 2$ RR, $T_{I1} + 3$ RR, $T_{I1} + 4$ RR, T_{I2} , $T_{I2} + 1$ RR, $T_{I2} + 2$ RR, $T_{I2} + 3$ RR, $T_{I2} + 4$ RR. [Color figure can be viewed in the online issue, which is available at wileyonlinelibrary.com.]

myocardium. 3D T_1 mapping has recently been proposed for volumetric LV coverage for postcontrast T_1 (25) and native T_1 (26). However, 3D T_1 mapping sequences still suffer from long scan times and require advanced reconstruction techniques, which are not yet clinically available. Therefore, currently, multiple separate 2D scans have to be performed for different slices to obtain complete LV coverage. This requires numerous breath-holds, which are not convenient for patients.

In this study, we propose a novel Slice-interleaved T_1 (STONE) sequence for free-breathing multislice inversion-recovery based T_1 mapping sequence with volumetric LV coverage by interleaving data acquisition of different slices during the recovery time of adjacent slices. The accuracy and precision of the proposed method is evaluated in numerical simulations, phantom and in vivo experiments and compared to T_1 mapping measurements using MOLLI.

METHODS

All imaging was performed on a 1.5 Tesla (T) scanner (Philips Achieva, Philips, Best, The Netherlands) with a 32-channel cardiac receiver coil array. The in vivo experiments were HIPAA compliant and approved by our Institutional Review Board. Written informed consent was obtained from each subject before the imaging.

Sequence

Figure 1 depicts the proposed STONE sequence, which enables T_1 measurements in five different slices simultaneously. At the beginning of the sequence, an

image with no magnetization preparation is acquired for each slice (Fig. 1a) to enable sampling of the fully recovered longitudinal magnetization. Subsequently, five inversion-recovery single-shot images are acquired after a single nonselective inversion pulse with an inversion time of T_{I1} which is defined as the time between the end of the adiabatic inversion pulse and the k-space center of the first slice (Fig. 1b). A total of five electrocardiogram (ECG)-triggered single-shot images are acquired with one image per each of the different slices, followed by a 3 s rest-period. Slice-selective excitation is used for the acquisition of each single-shot image, which ensures undisturbed longitudinal magnetization in the subsequent single-shot images acquired at different slice locations. The order of the slices, after the inversion pulses, is cycled-through, i.e., the acquisition block, consisting of an inversion pulse and five images, is repeated five times using the same inversion time but with a different slice order. This results in the acquisition of T_{I1} , $T_{I1} + 1$ RR, $T_{I1} + 2$ RR, $T_{I1} + 3$ RR, $T_{I1} + 4$ RR (RR describes the duration of one heart-beat) along the longitudinal recovery curve for each slice. Subsequently, the inversion time is changed and a similar data acquisition scheme is repeated with T_{I2} . In the end, for each slice, 11 T_1 -weighted images are acquired along the recovery curve sampled at ∞ , T_{I1} , $T_{I1} + 1$ RR, $T_{I1} + 2$ RR, $T_{I1} + 3$ RR, $T_{I1} + 4$ RR, T_{I2} , $T_{I2} + 1$ RR, $T_{I2} + 2$ RR, $T_{I2} + 3$ RR, $T_{I2} + 4$ RR. The typical scan time to cover five slices is 1:35 min for a heart-rate of 60 beats per min.

To enable coverage of all five slices and sufficient recovery time, the image acquisition is performed during free breathing. To reduce through-plane motion, we use

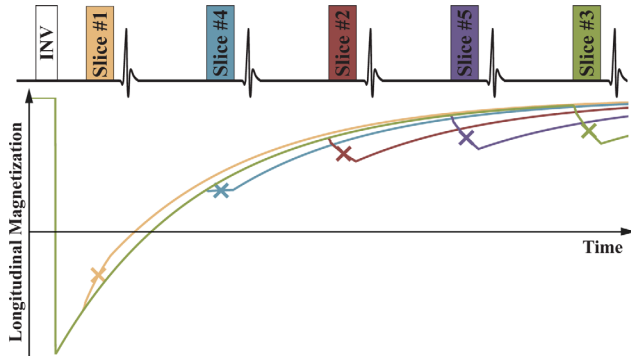


FIG. 2. Schematic of the longitudinal magnetization recovery in five different slices. The crosses indicate the acquisition time of the k-space centers. The magnetization in all slices is inverted with a nonselective inversion pulse. The subsequent image samplings only perturb the magnetization in a single-slice, while the other slices remain unperturbed. [Color figure can be viewed in the online issue, which is available at wileyonlinelibrary.com.]

prospective slice tracking using a pencil beam navigator positioned on the dome of the right hemidiaphragm. Spatially selective re-inversion at the navigator position is performed directly after each inversion pulse, to ensure a constant navigator signal across all inversion times. To minimize residual cross-talk, the slices are performed in a specific order after the inversion pulse, which maximizes the distance between two consecutive slices, as shown in Figure 1. The in-plane motion is compensated for by retrospective image registration using a nonrigid image registration algorithm for myocardial T_1 mapping (27). This algorithm simultaneously estimates a nonrigid motion field and intensity variations, and uses an additional regularization term to constrain the deformation field using automatic feature tracking.

Reconstruction

T_1 maps are generated by voxel-wise curve-fitting of the inversion-recovery signal-model to the image intensities. We propose to generate T_1 maps with two different signal models:

- A: Two-parameter fit model for the inversion recovery signal S_{2P} , defined by:

$$S_{2P}(t) = M_0(1 - 2e^{-\frac{t}{T_1}}), \quad [1]$$

where M_0 is the signal with full longitudinal magnetization recovery and T_1 the longitudinal relaxation time. The model assumes perfect inversion pulse efficiency and no disturbance of magnetization due to imaging pulses before the acquisition of the central k-space line.

- B: Three-parameter fit model for the inversion recovery signal S_{3P} , defined by:

$$S_{3P}(t) = M_0(1 - Be^{-\frac{t}{T_1}}), \quad [2]$$

with an additional parameter B , which models the apparent inversion efficiency. This was previously shown to

model imperfect inversion pulses, the recovery-curve disturbance caused by multiple RF excitations before the k-space center, and to reduce the susceptibility to magnetization transfer effects (16,20). Because the longitudinal magnetization recovery curve is only perturbed by one set of imaging pulses after the inversion (see Figure 2 for the signal recovery of five slices), no correction for disturbance by repeated imaging, as in MOLLI, is performed.

Numerical Simulations

Numerical simulations were performed to study the accuracy and precision of the STONE sequence for different combinations of T_1 and T_2 times. To simulate the impact of an imperfect RF inversion pulse on the accuracy and precision, the estimated T_1 was also calculated by varying the effective inversion flip angle. For comparison MOLLI with the 5-(3s)-3 scheme (17) was simulated. The Bloch equations were used to simulate the longitudinal and transverse magnetization curves for all sequences. T_1 times were generated from the simulated transverse magnetization at the echo time of the central k-space line using a two- and three-parameter fit model for the STONE sequence, and a three-parameter fit model with “flip-angle” correction for MOLLI (8,28).

The simulated sequences shared the following imaging parameters: balanced steady-state free precession (bSSFP) imaging readout, repetition time/echo time/ α (TR/TE/ α) = 2.9 ms / 1.54 ms / 35°, total phase-encoding lines = 70, linear k-space ordering, 10 linear sweep-up start-up pulses, heart-rate = 60 bpm. The resulting inversion times for the STONE sequence were: “ ∞ ”, 135, 1135, 2135, 3135, 4135, 350, 1350, 2350, 3350, 4350 ms and for the 5-(3s)-3 MOLLI: 135, 1135, 2135, 3135, 4135, 350, 1350, 2350 ms.

Two sets of simulations were performed. In the first set, the T_1 was varied between 400 and 1500 ms in steps of 100 ms, the T_2 time was varied between 35 and 65 ms in steps of 5 ms and the effective inversion flip-angle was kept constant as 180°. In the second set of simulations, the T_2 time was fixed to 50 ms, the T_1 time was varied between 400 and 1500 ms in steps of 100 ms, and the effective inversion flip-angle was changed from 150° to 180° in steps of 5°. Each simulation was performed 20,000 times with random Rician noise, corresponding to a signal-to-noise ratio (SNR) of 50 in the image with no magnetization preparation.

Accuracy was assessed as the absolute value of the difference between the simulated ground-truth T_1 time and the estimated T_1 time averaged over all repetitions. Precision was defined as the standard-deviation of the estimated T_1 time over the repetitions.

Phantom Imaging

A phantom study was performed to characterize the accuracy and precision of the estimated T_1 times measured with the STONE sequence. The phantom consisted of 9 vials containing NiCl₂-doped agarose-gel, with varying concentration resulting in T_1 times between 400 and 1600 ms and T_2 times between 50 and 200 ms. In addition to the STONE sequence, we acquired T_1 maps using

5-(3s)-3 MOLLI. A bSSFP imaging readout with the following sequence parameters was used for imaging: in-plane resolution = $2.1 \times 2.1 \text{ mm}^2$, slice thickness = 8 mm, field of view (FOV) = $360 \times 356 \text{ mm}^2$, TR/TE/ α = 2.9 ms / 1.54 ms / 35° , SENSE rate = 2, number of phase encoding lines = 78, linear k-space ordering, 10 linear sweep up pulses. An ECG signal was simulated with 60 bpm. Ten repetitions of each sequence were performed. The slice-gap in the STONE T_1 maps was 8 mm. For all three sequences, a slice-selective Sinc-Gauss RF excitation pulse with duration of 0.43 ms was used for imaging and an adiabatic hyperbolic-secant inversion pulse with 11 ms pulse-duration for magnetization preparation. MOLLI was performed with the acquisition of only one slice, aligned to the central slice of the STONE sequence. All DICOM images were exported and used for estimating the voxel-wise T_1 maps. The STONE T_1 maps were calculated using both two- and three-parameter fit models. MOLLI T_1 maps were generated by fitting a three-parameter fit model with additional correction for the disturbance from the repeated imaging pulses (28).

An inversion recovery spin-echo sequence (IR-SE) was used to measure reference T_1 values for each vial. Fifteen 2D IR-SE images were acquired using 15 different inversion times between 50 and 5000 ms with the following imaging parameters: in-plane spatial resolution = $1.3 \times 1.3 \text{ mm}^2$, slice-thickness = 8 mm, FOV = $120 \times 120 \text{ mm}^2$, TR/TE/ α = 10 s / 10 ms / 90° , and scan time = 3:20 h. Voxel-wise T_1 times were calculated off-line by fitting a three-parameter fit model to the 15 IR-SE images.

T_1 Analysis

For each method, the average T_1 time for each vial was measured as the average over a manually drawn region of interest (ROI) averaged over all repetitions. The accuracy was defined as the difference between the average T_1 time and the IR-SE T_1 . Precision was defined as the standard deviation of the estimated T_1 times in the ROI of all repetitions

In Vivo Imaging

We recruited seven healthy adult subjects (four males, age 28 ± 12 years), and seven patients (five males, age 64 ± 10 years) referred for clinical cardiac MR. The patient indications and symptoms leading to CMR were as follows: (i) A postpulmonary vein isolation (PVI) patient suffering from atrial fibrillation (AFib). (ii) A patient with left ventricular hypertrophy suffering from dyspnea, which was evaluated for infiltrative disease and hypertrophic cardiomyopathy. (iii) A patient with bicuspid aortic valve disease with a dilated aorta. (iv) A patient with a pericardial cyst, which was scanned for estimation of the cyst mass and chamber compression. (v) A coronary artery disease patient with new viral cardiomyopathy, evaluated for myocarditis. (vi) A cardiac sarcoidosis patient evaluated for scar assessment. (vii) A patient with palpitations and showing right ventricular dilation and trabeculations, which was scanned for evaluation of an arrhythmogenic right ventricle.

Each subject was imaged using two sequences: (i) STONE with five slices, (ii) 5-(3s)-3 MOLLI with three slices

acquired in three separate breath-holds. Both sequences were performed using a bSSFP read-out and the following parameters: in-plane resolution = $2.1 \times 2.1 \text{ mm}^2$, slice-thickness = 8 mm, FOV = $360 \times 352 \text{ mm}^2$, TR/TE/ α = 2.6 ms / 1.0 ms / 35° , SENSE-rate = 2, number of phase encoding lines = 78, linear ordering, 10 linear ramp-up start-up pulses. Five short-axis slices with 8 mm slice-gap were acquired with the STONE sequence, using a fixed respiratory navigator slice tracking factor of 0.6. Three slices, aligned to the central three slices of the STONE sequence, were acquired with MOLLI.

T_1 maps from the STONE sequence were generated using both two- and three-parameter fit models. MOLLI T_1 maps were generated with a three-parameter fit model and retrospective correction for the magnetization perturbation of the imaging pulses.

T_1 Measurements

An ROI was manually drawn in the septum for each method and each slice. All three slices were analyzed for MOLLI and only the corresponding central three slices for the STONE T_1 maps. The average T_1 time for a patient was assessed as the average T_1 within an ROI averaged over all slices. The mean of the standard deviation of the myocardial T_1 times within each ROI averaged over all slices was also calculated for each subject. T_1 times are also presented in an AHA 16 segment model (29). Manually drawn epi- and endocardial contours in the central three slices were used to segment the myocardium with reference to the insertion point of the right ventricle.

Statistical Analysis

The average T_1 time and the mean standard deviation within the myocardium of the three methods were statistically compared using a paired Student's t-test. A P -value of <0.05 was considered to be statistically significant. Furthermore, for the STONE method, the average T_1 times were analyzed across the slices. The hypothesis of no statistical significant difference between different slices was studied using a mixed-effects model analysis. Bonferroni correction was applied which results in a statistically significant threshold $P < 0.05 / 10 = 0.005$

RESULTS

Simulation

Accuracy

The accuracy of the three methods with varying simulated T_1 and T_2 times assuming perfect inversion-efficiency (top row), and with varying simulated T_1 times and inversion efficiency with constant T_2 of 50 ms (bottom row), are compared in Figure 3. The simulations show that, the multislice T_1 sequence with a three-parameter fit, results in the highest accuracy. The STONE sequence with a two-parameter fit model was more accurate than MOLLI. The deviation from the true T_1 time with MOLLI and the STONE sequence with a two-parameter fit increased with longer T_1 times, shorter T_2 times and worse inversion efficiency, resulting in an underestimation of up to 306 ms (MOLLI) and 176 ms

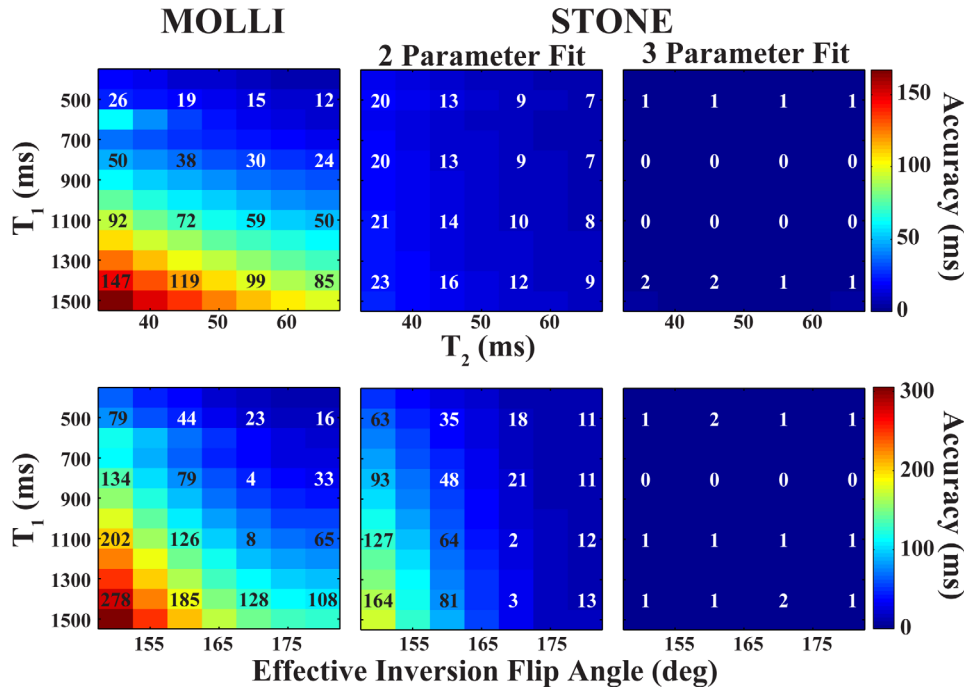


FIG. 3. Numerical simulations for calculating the accuracy of each T_1 sequence for various T_2 times assuming perfect inversion efficiency (top row) and effective inversion flip angle for a fixed T_2 time (bottom row). The accuracy was defined as the difference between the simulated T_1 times and the mean of all estimated T_1 times for one set of parameters. The STONE sequence with both the three-parameter and the two-parameter fit model shows improved accuracy compared to MOLLI. [Color figure can be viewed in the online issue, which is available at wileyonlinelibrary.com.]

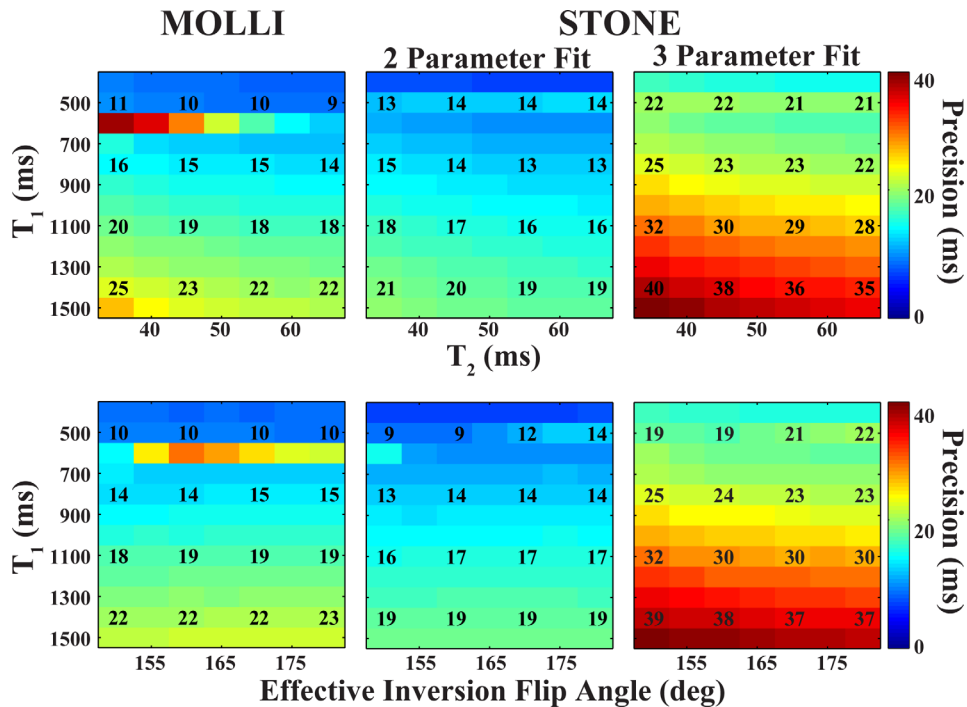


FIG. 4. Numerical simulations for calculating the precision of each T_1 sequence for different T_2 times assuming perfect inversion efficiency and various inversion efficiencies for a fixed T_2 time. The precision was assessed as the standard deviation over all estimated T_1 times for one set of parameters. The STONE sequence with a two-parameter fit and MOLLI show similar precision and both sequences yield better precision than the STONE sequence with a three-parameter fit. [Color figure can be viewed in the online issue, which is available at wileyonlinelibrary.com.]

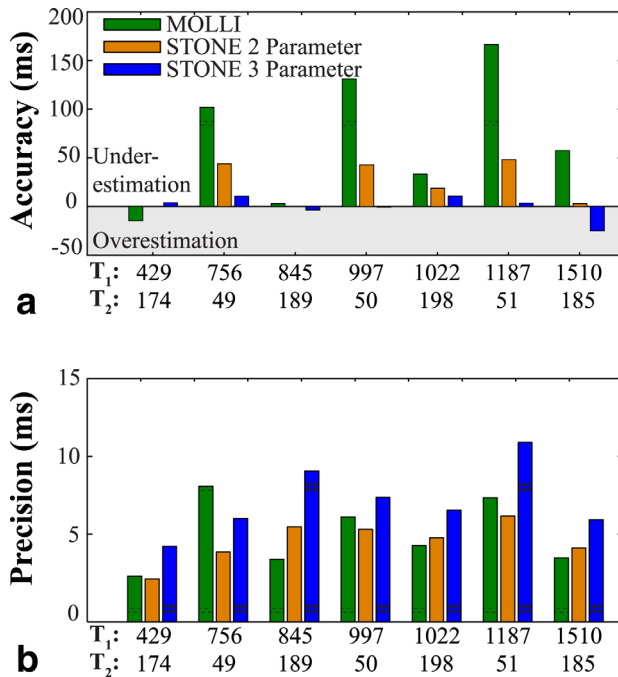


FIG. 5. Accuracy (a) and precision (b) of T₁ measurements in different phantom vials with different T₁ and T₂. Accuracy was defined as the difference between the average of all repetitions and a spin-echo inversion recovery reference T₁. Precision was assessed as the standard deviation of the estimated T₁ time across the vial and across the 10 repetitions. [Color figure can be viewed in the online issue, which is available at wileyonlinelibrary.com.]

(STONE two-parameter). The multislice with a three-parameter fit maintained T₁ times close to the spin-echo reference for all simulated ranges of T₁ and T₂ times (difference < 4 ms). The accuracy for parameters that can be expected for in vivo assessment of native T₁ times (T₁ ≈ 1200 ms, T₂ ≈ 50 ms, effective inversion flip-angle ≈ 160° [1]) was 145 ms with MOLLI, 70 ms and 0.1 ms with the STONE sequence using a two- and a three-parameter fit, respectively.

Precision

Figure 4 depicts the precision of the three methods in the simulation study with varying T₁ and T₂ times assuming

perfect inversion-efficiency (top row), and with varying T₁ times and inversion efficiency with constant T₂ of 50 ms (bottom row). The precision of all methods decreases with increasing T₁ and decreasing T₂, but with small variations for different inversion efficiencies in the numerical simulations. MOLLI and the STONE method with a two-parameter fit show increased precision compared to the STONE sequence with a three-parameter fit. The standard deviation of the estimated T₁ time for expected precontrast in vivo parameters (i.e., T₁ ≈ 1200 ms, T₂ ≈ 50 ms, effective inversion flip-angle ≈ 160° [1]) was 20 ms with MOLLI, 17 ms and 33 ms with STONE using a two- and a three-parameter fit, respectively.

Phantom

In Figure 5 the accuracy and precision of different T₁ mapping sequences in phantom experiments are shown. The STONE sequence with a two-parameter fit model resulted in significantly improved accuracy compared to MOLLI ($P < 0.001$). The deviation from the spin-echo sequence was decreased by an average of 52 ms (from 76 ± 58 ms using MOLLI to 23 ± 18 ms using STONE), which corresponded to an average relative accuracy improvement of 71%. STONE with a three-parameter fit model resulted in significantly more accurate T₁ times than the use of the two-parameter fit model ($P < 0.011$). The precision of MOLLI was similar to the STONE T₁ maps with a two-parameter fit model (4 ± 2 ms versus 4 ± 1 ms; $P = 0.62$), but better than three-parameter fit model (7 ± 2 ms; $P < 0.001$).

In Vivo

An exemplary, multislice STONE T₁ maps acquired in a healthy subject and reconstructed using a two- (top row) and a three-parameter (bottom row) fit model are shown in Figure 6. Visually improved T₁ map quality was observed with the two-parameter fit model. The same trend can be observed in the STONE T₁ maps acquired in patient subjects, as depicted in Figure 7. The effect of the in-plane image registration applied for respiratory motion compensation on a STONE multislice dataset is illustrated in Figure 8. Multiple T₁ weighted single-shot images acquired in one of the patient are shown before and after image registration. Despite substantial in-plane

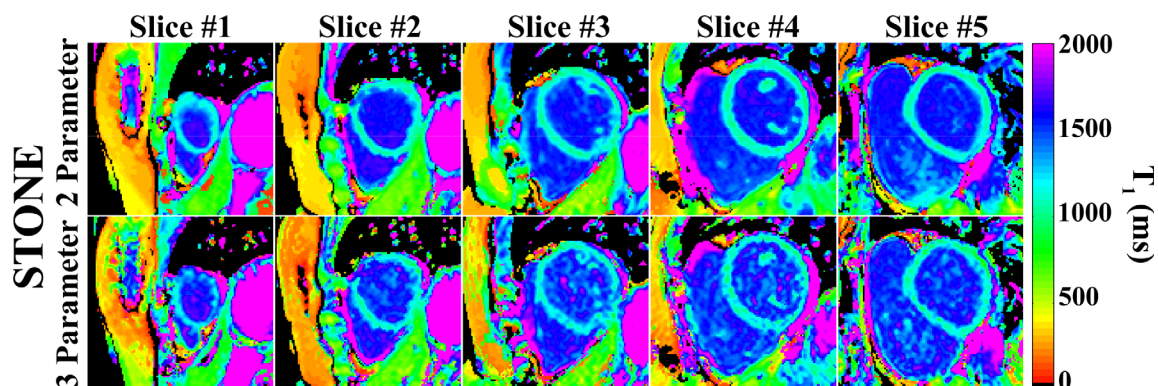


FIG. 6. Example multislice native T₁ maps acquired in a healthy subject using STONE, reconstructed using either a two- (top row) or three-parameter (bottom row) fit model. Visually improved T₁ map quality (i.e., lower signal variation across the myocardium) can be seen with the two-parameter fit model. [Color figure can be viewed in the online issue, which is available at wileyonlinelibrary.com.]

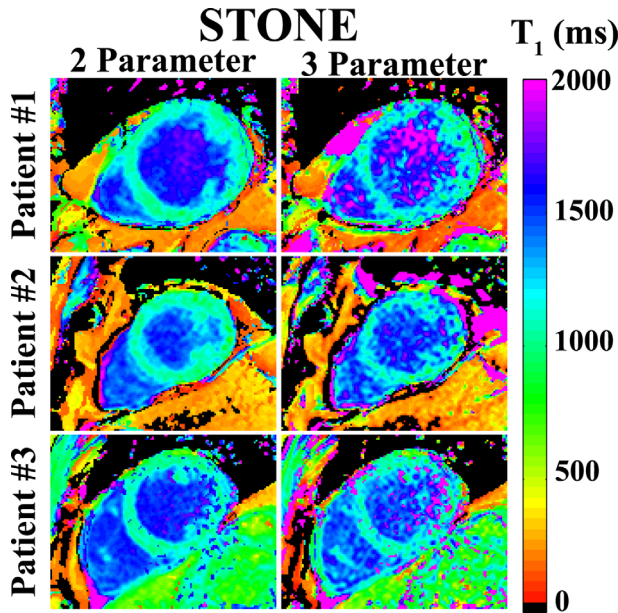


FIG. 7. Example T_1 maps in multiple patient subjects using the STONE technique reconstructed with two- and three-parameter fit model. Patient #1 was referred to CMR with coronary artery disease and viral cardiomyopathy, patient #2 with a pericardial cyst and patient #3 was a postpulmonary vein isolation (PVI) patient with atrial fibrillation. Visually improved T_1 map quality can be seen with two-parameter fit model, compared to a three-parameter fit model fit.

motion good spatial alignment of the myocardium is achieved in all slices after image registration. Figure 9 shows representative T_1 maps acquired with MOLLI and the STONE sequence in three different healthy subjects. Homogenous maps, with visually low noise contamination were obtained with MOLLI, and the STONE T_1

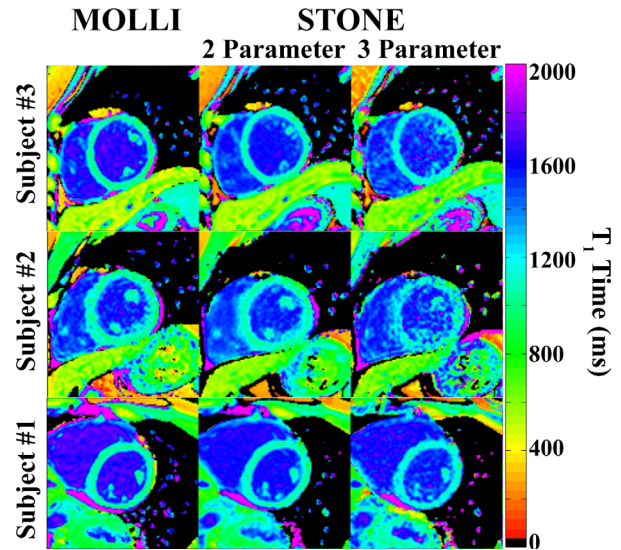


FIG. 9. Example native T_1 maps in three healthy adult subjects using MOLLI and the STONE sequence with two- and three-parameter fit model. Visually improved T_1 map quality can be seen with MOLLI and STONE with a two-parameter fit model, compared with a three-parameter fit model fit.

maps with a two-parameter fit model. The signal homogeneity decreased when using a three-parameter fit model with the STONE sequence.

Figure 10a summarizes the in vivo T_1 times measured in the healthy subjects and the patients with the three T_1 mapping methods. MOLLI consistently resulted in the lowest T_1 times: 1051 ± 33 ms for healthy subjects and 1092 ± 39 ms for patients. In vivo T_1 times with the STONE sequence using the two-parameter fit model were significantly longer for healthy subjects 1101 ± 27

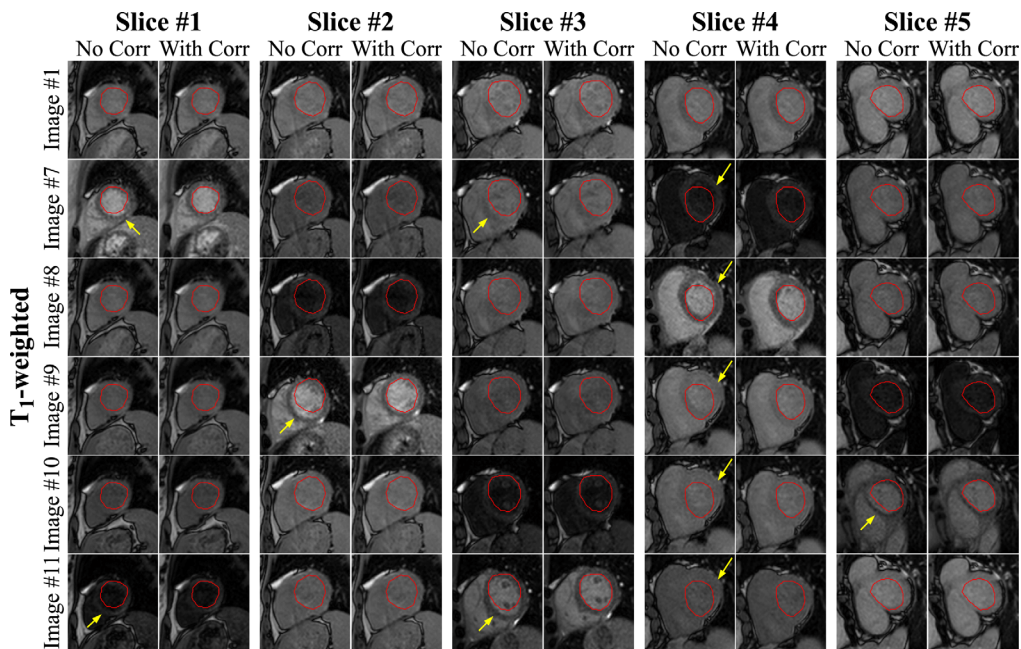


FIG. 8. Multislice dataset of T_1 -weighted images acquired with the STONE technique in a patient with right ventricular dilation and trabeculations before and after motion correction. The red endocardial border indicates the position of the myocardium in the reference Image #1. The arrows indicate images with substantial motion. Close agreement of the endocardial borders can be seen after the registration in all slices, and for all inversion times.

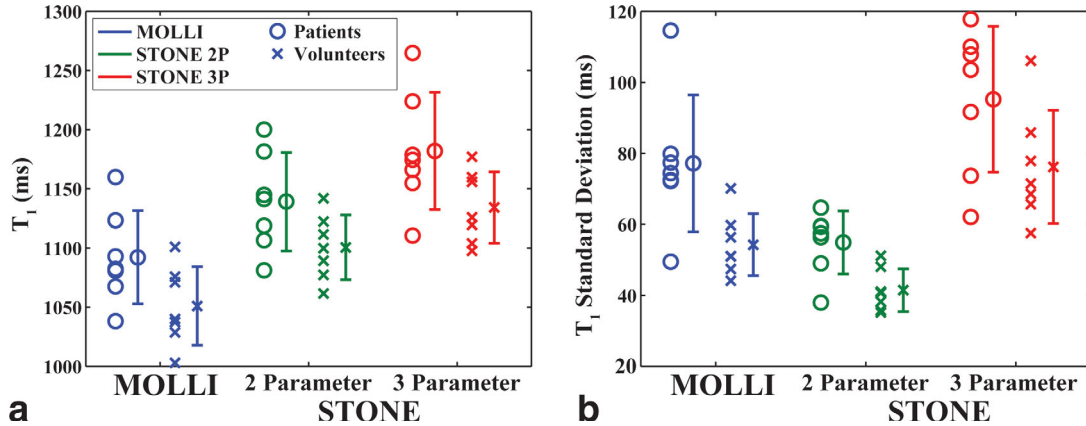


FIG. 10. The mean (a) and standard deviation (b) of T_1 times measured in the septum of 7 healthy subjects and 7 patients with suspected cardiac disease. The error bars indicate the mean and standard deviation for the T_1 across each cohort. MOLLI T_1 was lower than STONE with either two- or three-parameter fit model. The two-parameter fit yields lower T_1 compared to three-parameter fit model. The standard deviation of T_1 times in the septum was lower in the STONE sequence with two-parameter fit model compared to MOLLI or three-parameter fit model. [Color figure can be viewed in the online issue, which is available at wileyonlinelibrary.com.]

ms ($P < 0.01$) and for patients 1139 ± 42 ms ($P < 0.01$). The T_1 times assessed with the STONE sequence using the three-parameter fit model were significantly longer than with both of the former methods: 1134 ± 30 ms for healthy subjects ($P < 0.001$ versus MOLLI, $P < 0.02$ versus two-parameter) and 1182 ± 50 ms for patients ($P < 0.001$ for both MOLLI and two-parameter). With all methods, patient subjects showed a tendency of elevated T_1 times compared to healthy subjects. The average scan-time for the acquisition of five short-axis slices using STONE was $1:22 \pm 0:13$ min for the healthy subjects and $1:40 \pm 0:17$ min for the patients. This corresponds to an average scan-time per slice of 18 s including all necessary rest-periods. Figure 10b shows the standard deviation of the T_1 times within the septal ROI for all in vivo subjects. The lowest variations within the ROI were obtained using STONE with a two-parameter fit reconstruction: 41 ± 6 ms for healthy subjects and 55 ± 9 ms for patients. These variations were slightly increased to 54 ± 9 ms for healthy subjects and 77 ± 19 ms for patients using MOLLI. STONE with a three-parameter fit model showed the highest variations of T_1 times (76 ± 16 ms for healthy subjects, 95 ± 21 ms for patients). For all methods the variation in patients was higher indicating a lower T_1 map quality.

The T_1 maps acquired in the healthy subject from Figure 6, using the STONE sequence with a two- and three-parameter fit, are presented as a circumferential polar plot representation in Figure 11a. Visually high homogeneity was observed across the segments and across the slices. STONE in vivo T_1 times across the multiple slices are compared in Figure 11b. Pair-wise comparisons using the linear mixed model show no significant differences between STONE T_1 values in different slices using either the two-parameter or the three-parameter fit models ($P > 0.06$).

DISCUSSION

In this study, we proposed a novel multislice T_1 mapping sequence, called STONE, which provides more accurate T_1 times compared to the MOLLI sequence but with simi-

lar precision. Inversion-recovery based myocardial T_1 mapping sequences such as MOLLI have proven excellent precision and reproducibility. However, to overcome the problem of long rest-periods between the inversion pulses, the MOLLI scheme samples the longitudinal magnetization recovery curve multiple times after a single magnetization preparation pulse, which hinders the accuracy. In the proposed scheme the rest-periods between the inversion-pulses are used for slice-selective

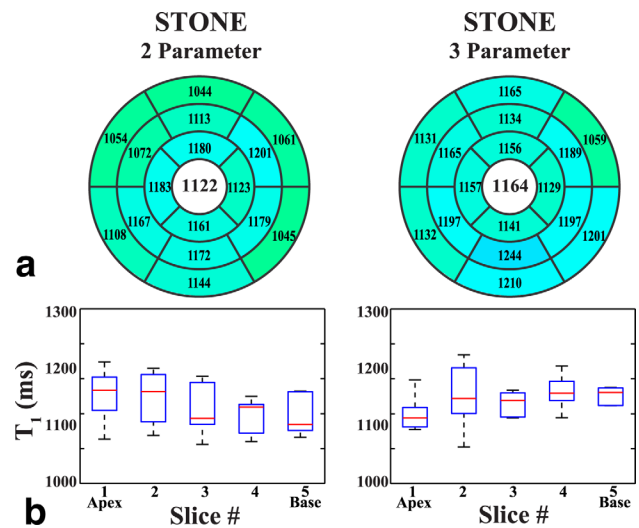


FIG. 11. a: The circumferential polar plot of the T_1 times in 16 myocardial segments according to AHA model, as well as the average over the whole myocardium (bold number in the center on white background) measured in a healthy adult subject with the STONE sequence with two- and three-parameter fit. b: T_1 times across all five slices for the healthy subjects measured using the STONE sequence. The red-line indicates the mean T_1 time for each slice across all subjects (healthy and patients). The box indicates the position of the 25th and 75th quartile, while the whiskers show the range of observed T_1 times. No statistically significant difference was found in the pair-wise comparisons between different slices using either the two-parameter or the three-parameter fit models ($P > 0.06$). [Color figure can be viewed in the online issue, which is available at wileyonlinelibrary.com.]

imaging of other slices. This allows for sampling of an undisturbed magnetization recovery curve without the need for extensive rest-periods, resulting in a scan-time of less than 20 s per slice, while not requiring a correction for the disturbance of the imaging pulses of a repeated imaging read-out.

Residual disturbance of the longitudinal magnetization might be induced by the excitation in neighboring slices, due to imperfect slice-profiles, residual respiratory motion or cardiac motion. To minimize the through-plane motion, prospective slice tracking using a respiratory navigator was performed and the slice ordering was chosen to maximize the distance between slices in successive heartbeats. We used an 8 mm slice gap with five slices to minimize the potential cross-talk effects. We arbitrarily chose the number and location of the sampling points on the T_1 recovery curve to parallel that of a MOLLI sequence. Different number of sampling points or slices, allowing for increased slice-gap, may be achieved by a slight modification of the imaging sequence, but this was not studied.

Respiratory and cardiac motion are known to be major detrimental factors for the quality of myocardial T_1 maps. As previously proposed methods, including MOLLI, the proposed STONE technique is based on parallel imaging accelerated 2D single-shot images with an acquisition window length of approximately 200 ms. Hence, the proposed technique is equally susceptible to blurring induced in the single-shot images by cardiac motion during the acquisition window. However, as the proposed technique is performed during free-breathing, heavy respiratory motion during the acquisition window can potentially lead to an increased level of blurring in the single-shot images compared to MOLLI.

The SSFP startup pulses and acquisition of multiple k-space lines in the linear ordering disturb the longitudinal magnetization before the central k-space line is acquired. However, it has been shown that the effect of pulses in single-shot bSSFP imaging, as used in most recent T_1 mapping sequences, on the longitudinal magnetization can be modeled as an affine transformation (30). Hence, the accuracy is maintained if a three-parameter fit model is used. However, if a two-parameter fit model is used these pulses induce dependence on the T_2 time, the flip-angle and the TR (20), as well as the inversion-efficiency. As the numerical simulations and the phantom experiments show, this loss in accuracy with the proposed sequence is considerably lower than for the case of repeated imaging of a disturbed longitudinal magnetization used in MOLLI. As shown in Kellman and Hansen (31) and observed in this study, a fit with the two-parameter fit model provides a significant gain of precision with a trade-off of decreased accuracy.

The flip-angle was chosen as 35° for the proposed sequence to minimize the loss in accuracy if a two-parameter fit model is used for reconstruction. A higher flip-angle causes greater disturbance of the magnetization before the acquisition of the central k-space line. Hence, if STONE is used with the two-parameter fit model in this case, the accuracy of the method will be impaired. On the other hand, a higher flip-angle leads to an improved image SNR, resulting in better precision. Hence, if STONE is used with a three-parameter fit

model only, the application of a high flip-angle may increase the precision, without impairing the accuracy, if sufficient rest-periods are inserted. Further studies in optimizing the flip angle are needed to investigate the trade-off between accuracy and precision for the proposed STONE sequence.

A phase-sensitive reconstruction has previously been proposed for MOLLI T_1 mapping (32). In this reconstruction the phase information is used to restore the signal polarity of the magnitude images before the T_1 fit, eliminating the need for integrated polarity restoration based on the fit residual. This was shown to increase the precision of inversion recovery based T_1 mapping sequences. The phase-maps of the 2D single-shot images acquired with the STONE technique, can be spatially registered using the deformation maps obtained in the magnitude image registration. This potentially allows for phase-information based polarity restoration and the application of the phase-sensitive reconstruction technique. Future research is warranted to study the increase in precision using a phase-sensitive reconstruction in STONE.

For the in vivo T_1 time analysis, the standard deviation of the T_1 times within a septal ROI was used as a surrogate for the in vivo precision. This measure is highly susceptible to the positioning of the ROI, partial voluming effects and artifacts. Hence, its use as a surrogate for the noise-resilience of a T_1 mapping technique is limited.

The accuracy of the T_1 times could not be compared in vivo as there is currently no feasible method for the acquisition of reference T_1 times in the myocardium available. However, careful evaluations in simulations and phantom measurements indicate improved accuracy with the proposed technique. Furthermore, STONE results in longer in vivo T_1 times than MOLLI, which is known to underestimate the native T_1 values (14).

The proposed method was implemented and tested on a 1.5T scanner only. Higher magnetic field strength may be advantageous for myocardial T_1 mapping due to higher SNR, which can improve the precision of the T_1 maps. Improved SNR will also enable shortened acquisition window lengths of the single-shot images which reduces the impact of cardiac motion. However, bSSFP imaging at 3T may also result in increased artifacts due to off-resonance. Furthermore, achieving perfect inversion-pulses will be more challenging, which could impact accuracy of the measurement using a two-parameter fit-model. Comprehensive evaluation of this technique at 3T is warranted.

Although the sequence can be applied for postcontrast T_1 mapping, this was not analyzed in the current study. The precise estimation of short postcontrast T_1 times may require a denser sampling of short-inversion times. With the STONE sequence, this can be achieved by reducing the number of slices, and increasing the number of imaging sets by varying the TI. In addition to post-contrast T_1 of myocardium, the blood T_1 is also needed for calculation of ECV. For blood T_1 , the impact of inflow saturation and disturbance of the inflowing blood need to be taken into account. However for blood T_1 , usually only a single value is needed. Further studies are warranted to investigate the accuracy and precision of ECV calculation for the STONE sequence.

CONCLUSIONS

The STONE sequence allows accurate and precise estimation of native myocardial T_1 times over multiple slices.

ACKNOWLEDGMENT

Sebastian Weingärtner is supported by a fellowship from the Deutsche Telekom Stiftung.

REFERENCES

- Kellman P, Herzka DA, Hansen MS. Adiabatic inversion pulses for myocardial T_1 mapping. *Magn Reson Med* 2013;71:1428–1434.
- Messroghli DR, Walters K, Plein S, Sparrow P, Friedrich MG, Ridgway JP, Sivananthan MU. Myocardial T_1 mapping: application to patients with acute and chronic myocardial infarction. *Magn Reson Med* 2007;58:34–40.
- Mewton N, Liu CY, Croisille P, Bluemke D, Lima JAC. Assessment of myocardial fibrosis with cardiovascular magnetic resonance. *J Am Coll Cardiol* 2011;57:891–903.
- Ng ACT, Auger D, Delgado V, et al. Association between diffuse myocardial fibrosis by cardiac magnetic resonance contrast-enhanced T_1 mapping and subclinical myocardial dysfunction in diabetic patients: a pilot study. *Circ Cardiovasc Imaging* 2012;5:51–59.
- Iles L, Pfluger H, Phrommintikul A, Cherayath J, Aksit P, Gupta SN, Kaye DM, Taylor AJ. Evaluation of diffuse myocardial fibrosis in heart failure with cardiac magnetic resonance contrast-enhanced T_1 mapping. *J Am Coll Cardiol* 2008;52:1574–1580.
- Sibley CT, Noureldin RA, Gai N, et al. T_1 Mapping in cardiomyopathy at cardiac MR: comparison with endomyocardial biopsy. *Radiology* 2012;265:724–732.
- Arheden H, Saeed M, Higgins CB, Gao DW, Bremerich J, Wyttenbach R, Dae MW, Wendland MF. Measurement of the distribution volume of gadopentetate dimeglumine at echo-planar MR imaging to quantify myocardial infarction: comparison with ^{99m}Tc -DTPA autoradiography in rats. *Radiology* 1999;211:698–708.
- Messroghli DR, Radjenovic A, Kozierke S, Higgins DM, Sivananthan MU, Ridgway JP. Modified Look-Locker inversion recovery (MOLLI) for high-resolution T_1 mapping of the heart. *Magn Reson Med* 2004;52:141–146.
- Messroghli DR, Plein S, Higgins DM, Walters K, Jones TR, Ridgway JP, Sivananthan MU. Human myocardium: single-breath-hold MR T_1 mapping with high spatial resolution - reproducibility study. *Radiology* 2006;238:1004–1012.
- Kawel N, Nacif M, Zavodni A, Jones J, Liu S, Sibley C, Bluemke D. T_1 mapping of the myocardium: intra-individual assessment of post-contrast T_1 time evolution and extracellular volume fraction at 3T for Gd-DTPA and Gd-BOPTA. *J Cardiovasc Magn Reson* 2012;14:26.
- Rogers T, Dabir D, Mahmoud I, Voigt T, Schaeffter T, Nagel E, Puntmann VO. Standardization of T_1 measurements with MOLLI in differentiation between health and disease - the ConSept study. *J Cardiovasc Magn Reson* 2013;15:78.
- Raman FS, Kawel-Boehm N, Gai N, Freed M, Han J, Liu CY, Lima JA, Bluemke DA, Liu S. Modified look-locker inversion recovery T_1 mapping indices: assessment of accuracy and reproducibility between magnetic resonance scanners. *J Cardiovasc Magn Reson* 2013;15:64.
- Kellman P, Herzka DA, Arai AE, Hansen MS. Influence of Off-resonance in myocardial T_1 -mapping using SSFP based MOLLI method. *J Cardiovasc Magn Reson* 2013;15:63.
- Piechnik S, Ferreira V, Dall'Armellina E, Cochlin L, Greiser A, Neubauer S, Robson M. Shortened Modified Look-Locker Inversion recovery (ShMOLLI) for clinical myocardial T_1 -mapping at 1.5 and 3 T within a 9 heartbeat breathhold. *J Cardiovasc Magn Reson* 2010;12:69.
- Chow K, Flewitt J, Pagano J, Green J, Friedrich M, Thompson R. T_2 -dependent errors in MOLLI T_1 values: simulations, phantoms, and in-vivo studies. *J Cardiovasc Magn Reson* 2012;14:1–2.
- Robson MD, Piechnik SK, Tunnicliffe EM, Neubauer S. T measurements in the human myocardium: the effects of magnetization transfer on the SASHA and MOLLI sequences. *Magn Reson Med* 2013;70:664–670.
- Kellman P, Arai AE, Xue H. T_1 and extracellular volume mapping in the heart: estimation of error maps and the influence of noise on precision. *J Cardiovasc Magn Reson* 2013;15:56.
- Roujol S, Weingartner S, Foppa M, Chow K, Kawaji K, Ngo L, Kellman P, Manning WJ, Thompson RB, Nezafat R. Accuracy and reproducibility of four T_1 mapping sequences: A head-to-head comparison of MOLLI, ShMOLLI, SASHA, and SAPPHERE. *Radiology* 2014. doi: 10.1148/radiol.14140296.
- Higgins DM, Ridgway JP, Radjenovic A, Sivananthan UM, Smith MA. T_1 measurement using a short acquisition period for quantitative cardiac applications. *Med Phys* 2005;32:1738–1746.
- Chow K, Flewitt JA, Green JD, Pagano JJ, Friedrich MG, Thompson RB. Saturation recovery single-shot acquisition (SASHA) for myocardial T mapping. *Magn Reson Med* 2014;71:2082–2095.
- Weingärtner S, Akcakaya M, Basha T, Kissinger KV, Goddu B, Berg S, Manning WJ, Nezafat R. Combined saturation/inversion recovery sequences for improved evaluation of scar and diffuse fibrosis in patients with arrhythmia or heart rate variability. *Magn Reson Med* 2014;71:1024–1034.
- Puntmann VO, D'Cruz D, Smith Z, Pastor A, Choong P, Voigt T, Carr-White G, Sangle S, Schaeffter T, Nagel E. Native myocardial T_1 mapping by cardiovascular magnetic resonance imaging in subclinical cardiomyopathy in patients with systemic lupus erythematosus. *Circ Cardiovasc Imaging* 2013;6:295–301.
- Ellims AH, Iles LM, Ling LH, Hare JL, Kaye DM, Taylor AJ. Diffuse myocardial fibrosis in hypertrophic cardiomyopathy can be identified by cardiovascular magnetic resonance, and is associated with left ventricular diastolic dysfunction. *J Cardiovasc Magn Reson* 2012;14:76.
- Lu M, Zhao S, Yin G, et al. T_1 mapping for detection of left ventricular myocardial fibrosis in hypertrophic cardiomyopathy: a preliminary study. *Eur J Radiol* 2013;82:e225–e231.
- Weingärtner S, Akcakaya M, Roujol S, Basha T, Stehning C, Kissinger KV, Goddu B, Berg S, Manning WJ, Nezafat R. Free-breathing post-contrast three-dimensional T_1 mapping: volumetric assessment of myocardial T_1 values. *Magn Reson Med* 2014. doi: 10.1002/mrm.25124.
- Clique H, Cheng H-LM, Marie P-Y, Felblinger J, Beaumont M. 3D myocardial T_1 mapping at 3T using variable flip angle method: pilot study. *Magn Reson Med* 2014;71:823–829.
- Roujol S, Foppa M, Weingartner S, Manning WJ, Nezafat R. Adaptive registration of varying contrast-weighted images for improved tissue characterization (ARCTIC): Application to T_1 mapping. *Magn Reson Med* 2014. doi: 10.1002/mrm.25270.
- Deichmann R, Haase A. Quantification of T_1 values by SNAPSHOT-FLASH NMR imaging. *J Magn Reson* 1992;96:608–612.
- Cerqueira MD, Weissman NJ, Dilsizian V, Jacobs AK, Kaul S, Laskey WK, Pennell DJ, Rumberger JA, Ryan T, Verani MS. Standardized myocardial segmentation and nomenclature for tomographic imaging of the heart. A statement for healthcare professionals from the Cardiac Imaging Committee of the Council on Clinical Cardiology of the American Heart Association. *Circulation* 2002;105:539–542.
- Scheffler K. On the transient phase of balanced SSFP sequences. *Magn Reson Med* 2003;49:781–783.
- Kellman P, Hansen MS. T_1 -mapping in the heart: accuracy and precision. *J Cardiovasc Magn Reson* 2014;16:2.
- Xue H, Greiser A, Zuehlsdorff S, Jolly M-P, Guehring J, Arai AE, Kellman P. Phase-sensitive inversion recovery for myocardial T_1 mapping with motion correction and parametric fitting. *Magn Reson Med* 2013;69:1408–1420.